A&A 569, A78 (2014)
DOI: 10.1051/0004-6361/201424285

Astronomy & Astrophysics

A 52 hours VLT/FORS2 spectrum of a bright $z \sim 7$ HUDF galaxy: no Ly-α emission⋆

E. Vanzella[1], A. Fontana[2], L. Pentericci[2], M. Castellano[2], A. Grazian[2], M. Giavalisco[3], M. Nonino[4], S. Cristiani[4], G. Zamorani[1], and C. Vignali[5]

[1] INAF – Osservatorio Astronomico di Bologna, via Ranzani 1, 40127 Bologna, Italy
e-mail: eros.vanzella@oabo.inaf.it
[2] INAF – Osservatorio Astronomico di Roma, via Frascati 33, 00040 Monteporzio, Italy
[3] Department of Astronomy, University of Massachusetts, 710 North Pleasant Street, Amherst, MA 01003, USA
[4] INAF – Osservatorio Astronomico di Trieste, via G. B. Tiepolo 11, 34131 Trieste, Italy
[5] Dipartimento di Fisica e Astronomia, Universita' degli Studi di Bologna, Viale Berti-Pichat 6/2, 40127 Bologna, Italy

Received 27 May 2014 / Accepted 11 July 2014

ABSTRACT

Aims. We aim to determine the redshift of GDS_1408, the most solid $z \sim 7$ galaxy candidate lying in the *Hubble* Ultra Deep Field.
Methods. We have used all the VLT spectra for GDS_1408 that has been collected by two other groups with FORS2 at VLT and by us in the last five years for a total integration time of 52 h. The combined spectrum is the deepest ever obtained of a galaxy in the reionization epoch.
Results. We do not detect any emission line or continuum up to 10 100 Å. Based on an accurate set of simulations, we are able to put a stringent upper limit of $f(\mathrm{Ly}\alpha) < 3\times10^{-18}$ erg/s/cm^2 at 3–9 sigma in the explored wavelength range, which corresponds to a rest-frame equivalent width $EW < 9$ Å. Combining this limit with the spectral energy distribution (SED) modeling, we refine the redshift to be $z = 6.82 \pm 0.1$ (1-sigma). The same SED fitting indicates that GDS_1408 is relatively extinct ($A_{1600} \simeq 1$) with a dust corrected star-formation rate of $\simeq$20 $M_\odot$ yr^{-1}. The comparison between the un-attenuated equivalent width predicted by the case-B recombination theory and the observed upper limit provides a limit on the effective Lyα escape fraction of $f_{\rm esc}^{\rm eff}(\mathrm{Ly}\alpha) < 8\%$. Even though we cannot rule out a major contribution of the inter/circum galactic medium in damping the line, a plausible interpretation is that G2_1408 is moderately evolved and contains sufficient gas and dust to attenuate the Lyα emission before it reaches the intergalactic medium.
Conclusions. The redshift confirmation of even the best $z \simeq 7$ candidates is very hard to achieve (unless the Lyα or unusually strong rest-UV nebular emission lines are present) with the current generation of 8–10 m class telescopes. We show that both JWST and E-ELT are necessary to make decisive progresses. Currently, the increased redshift accuracy obtained with this kind of analysis makes ALMA an interesting option for the redshift confirmation.

Key words. galaxies: high-redshift – galaxies: formation – galaxies: distances and redshifts

1. Introduction

Understanding the process of reionization of the intergalactic medium (IGM) in the early Universe and the nature of the first galaxies responsible for that process are among the most important goals of modern cosmology (Robertson et al. 2010, and references therein). Thanks to deep and panchromatic data, such as GOODS, CANDELS and *Hubble* Ultra Deep Field (HUDF), great progress has been made in our ability to identify and subsequently confirm (spectroscopically) galaxies at $z < 7$. The most prominent spectral feature in the UV rest-frame wavelengths probed by optical/NIR spectroscopy at $z \simeq 7$ is the Lyα emission line (e.g., Vanzella et al. 2011, V11; Pentericci et al. 2011, 2014; P11, P14; Schenker et al. 2012, 2014; Ono et al. 2012; Shibuya et al. 2012). However, at $z > 7$ the situation is still challenging and only a handful objects are spectroscopically secured at present. There are at least two main reasons: (1) Physical processes in the galaxies: the Lyα emission is a resonant atomic transition that is very sensitive to dust attenuation and can be used as a diagnostic of the physical processes occurring within the galaxy (Giavalisco et al. 1996; Atek et al. 2014), since its strength and velocity profile depend on the instantaneous star formation rate, gas and dust content, metallicity, kinematics, and geometry of the interstellar medium. Therefore, an evolution of the average galaxy properties with time (gas and/or dust properties and/or ionizing emission) can make it intrinsically absent at specific cosmic epochs. (2) Reionization: the Lyα emission line may suffer a damping effect due to an increase of the neutral gas fraction in the IGM and/or circumgalactic medium (CGM; Miralda-Escudé et al. 2000; Dijkstra et al. 2011; Treu et al. 2012) or an increasing incidence of optically thick absorption systems (Bolton & Haehnelt 2013) as the ending phase of the reionization is approached. Another limiting effect was instrumental: efficient near-infrared spectrographs ($\lambda \gtrsim 1$ μm) with multiplexing capabilities are needed to capture UV rest-frame features for many targets at once, and they are becoming available only recently (e.g., VLT/KMOS, Keck/MOSFIRE, LBT/LUCI).

While point (1) is alleviated in that (on average) the frequency of Lyα line emitters appear to increase as redshift increases ($3 < z < 6.5$, Ouchi et al. 2008; Schaerer et al. 2011; Stark et al. 2011), the damping due to reionization may severely limit our current ability to confirm galaxies at $7 < z < 10$ (but

⋆ This work is based on data collected at ESO VLT (prog.ID 084.A-0951(A), 086.A-0968(A), 088.A-1013(A) and 088.A-1008(A)) and at NASA HST.

see Dijkstra & Wyithe 2010). Finkelstein et al. (2013) find only one galaxy at $z = 7.51$ out of 43 candidates at $z > 6.5$ with the Keck/MOSFIRE. Similarly, Schenker et al. (2014) find only one possible Lyα line at $z = 7.62$ in their sample of 19 $z \sim 8$, remarking that some process is making the Lyα difficult to detect. Therefore, there is a large fraction of non-Lyα emitters lying well within the first Gyr after the Big-Bang, whose nature is worth investigating. Clearly, all these explainations assume that the efficiency of the color selection based on the Lyα-break remains extremely high at $z \geq 7$, where the most current $z \geq 7$ candidates are indeed at their estimated redshifts.

In this work, we report on an ultradeep spectrum (52 h integration) of the brightest $z \simeq 7$ galaxy in the HUDF ($F125W = 26.1 \pm 0.02$). Being by far the brightest $z \simeq 7$ candidate in this well-studied region, it has been continuously selected as a high redshift candidate from the earliest NICMOS to the current ultradeep HUDF data at a variance with other targets (Yan & Windhorst 2004; Bouwens et al. 2004, 2008, 2011, 2014; Bouwens & Illingworth 2006; Labbé et al. 2006; Oesch et al. 2010; Fontana et al. 2010; McLure et al. 2010, 2013; Bunker et al. 2010; Yan et al. 2010; Finkelstein et al. 2010; Castellano et al. 2010; Wilkins et al. 2011; Grazian et al. 2011). We focus here on the combination of ultradeep spectroscopy and photometry to derive new insights about its nature.

Errors are quoted at the 1σ confidence level unless otherwise stated. Magnitudes are given in the AB system (AB $\equiv 31.4 - 2.5 \log\langle f_\nu/\mathrm{nJy}\rangle$). We assume a cosmology with $\Omega_{\rm tot}, \Omega_{\rm M}, \Omega_\Lambda = 1.0, 0.3, 0.7$ and $H_0 = 70$ km s^{-1} Mpc^{-1}.

2. FORS2 observations and data reduction

The HUDF-J033242.56-274656.6 galaxy (G2_1408 in Castellano et al. 2010 and hereafter) has been observed through four different VLT/FORS programs collected in the period 2009-2012: 084.A-0951(A) (P.I. Fontana), 086.A-0968(A) – 088.A-1013(A) (P.I. Bunker), 088.A-1008(A) (P.I. Bouwens), and 283.A-5063 (P.I. Carollo) with exposure times of 18 (Fontana, F18), 27 (Bunker, B27), 7 (Bouwens, B7) and 8 (Carollo, C8) hours on target, respectively, for a total of ≃60 h integration time. Unfortunately, in the program 283.A-5063, the G2_1408 source was placed at a position where the CCD has a defect, and no dithering has been performed; therefore, we exclude the 283.A-5063 program from the following analysis. The total usable exposure time is 52 h. The median seeing was ∼0.8 arcsec in all runs. The F18 data were presented in Fontana et al. (2010) where we reported a tentative detection of a Lyα line at $z = 6.972$. The other runs, B27 and B7, have been obtained subsequently in many different nights (especially B27), and particular care has been devoted to the alignments of the frames by using bright sources and sky emission lines. The B27 program has also been presented in Caruana et al. (2014), where they reported a $S/N \simeq 3.2$ at the location of the putative Lyα at $z = 6.972$. We discuss any possible presence of Lyα emission by combining all the available programs in detail.

Data reduction has been performed as in Vanzella et al. (2011), with particular care to the sky subtraction. The classical "A-B" dithering scheme that combines the partial frames (A-B) and (B-A) is performed with an additional treatment that *equalizes for* local differences in the number counts between frames (e.g., due to time variation of sky lines, distortion, etc.). The algorithm implements an "A-B" sky subtraction joined with a zero (e.g., median) or first order fit of the sky along columns that regularized possible local differences in the sky counts among the partial frames before they are combined. Finally, the two-dimensional spectra have been combined with a weighted average, and the subsequent resulting spectrum has been flux and wavelength calibrated. The two dimensional sky-subtracted partial frames are also combined (in the pixel domain) to produce the weighted RMS map, which is associated to the final reduced spectrum. This allows us to calculate the two-dimensional signal to noise (S/N) spectra, which is useful to access the reliability of the spectral features (as we address below with simulations).

Further checks have been performed on other targets placed in the masks and on those in common between F18 and B27. In particular, Caruana et al. (2014) targeted the same faint i-band dropout we confirmed previously with F18 (Fontana et al. 2010), GDS J033229.41-274537.8 at $z = 5.927$. While the continuum is not detected in the F18 spectrum, we find a very faint trace redward of the line in our B27 spectrum and a Lyα with an estimated flux of 3.8×10^{-18} erg/s/cm^2 at $S/N \simeq 8$, which is about a factor 1.25 higher than F18, whose flux is estimated to be $\simeq 3.0 \times 10^{-18}$ erg/s/cm^2 with $S/N \simeq 6.5$. Both flux and error estimates are compatible within the flux calibration accuracy and different integration time. The top part of Fig. 1 shows the S/N spectra of the $z = 5.927$ galaxy (i.e., the reduced spectrum divided by its rms map).

Following the above approach, we have combined the 52 h of observations of GDS_1408. The three individual S/N spectra and the conbined one are shown in the bottom part of Fig. 1. The 52 h spectrum is the deepest spectroscopic observation of a $z \sim 7$ galaxy obtained to date.

3. Results

Before discussing any feature in the spectrum, we note that the available photometry already constrains the redshift in the range ($6.5 < z < 7.0$) where FORS2 is an efficient instrument for the detection of the corresponding Lyα in both terms of wavelength coverage and response. First, we recall that the high redshift-nature ($z > 6.5$) is guaranteed by the large observed break between the ultradeep optical and near-infrared bands ($\Delta m \simeq 4$ mag) globally and the well-determined flat behavior of the SED in the near-infrared bands, as detected with a high S/N (HST-WFC3, $S/N \simeq 20$–50), as shown in Figs. 2 and 3. This makes GDS_1408 one of the most robust $z \sim 7$ candidates. Second, a reliable upper limit on the redshift is provided by the clear detections in the z_{850} band ($z < 7.3$) and narrow band filter, NB973 ($z < 7$), which is centered at $\lambda = 9755$ Å and d$\lambda = 200$ Å (Fig. 3). The limit provided with the 3σ detection in the NB973 is $z < 6.94$ if the entire *NB973* filter is capturing the galaxy continuum, $z_{\rm MAX} = (9755 - 100)/1215.7 - 1 = 6.94$ (see inset of Fig. 3).

3.1. A deep upper limit to the Lyα flux

Given the above upper limit $z_{\rm MAX}$, the FORS2 + 600z configuration provides a safe constraint on the Lyα line flux[1]. Indeed, there are no obvious spectral features in the three S/N spectra at the position of the G2_1408 (marked by arrows) nor in the combined one (see Fig. 1).

We note that these deeper data do not confirm the tentative detection of a weak line located at $\lambda = 9691.5 \pm 0.5$ Å,

[1] As an example, Fig. 1 shows the secondary object in B7 spectrum in which the Hα line is detected at $z = 0.535$ consistently with the zphot = 0.5 and shows that the FORS2 + 600z configuration is still performing well at ∼10 100 Å.

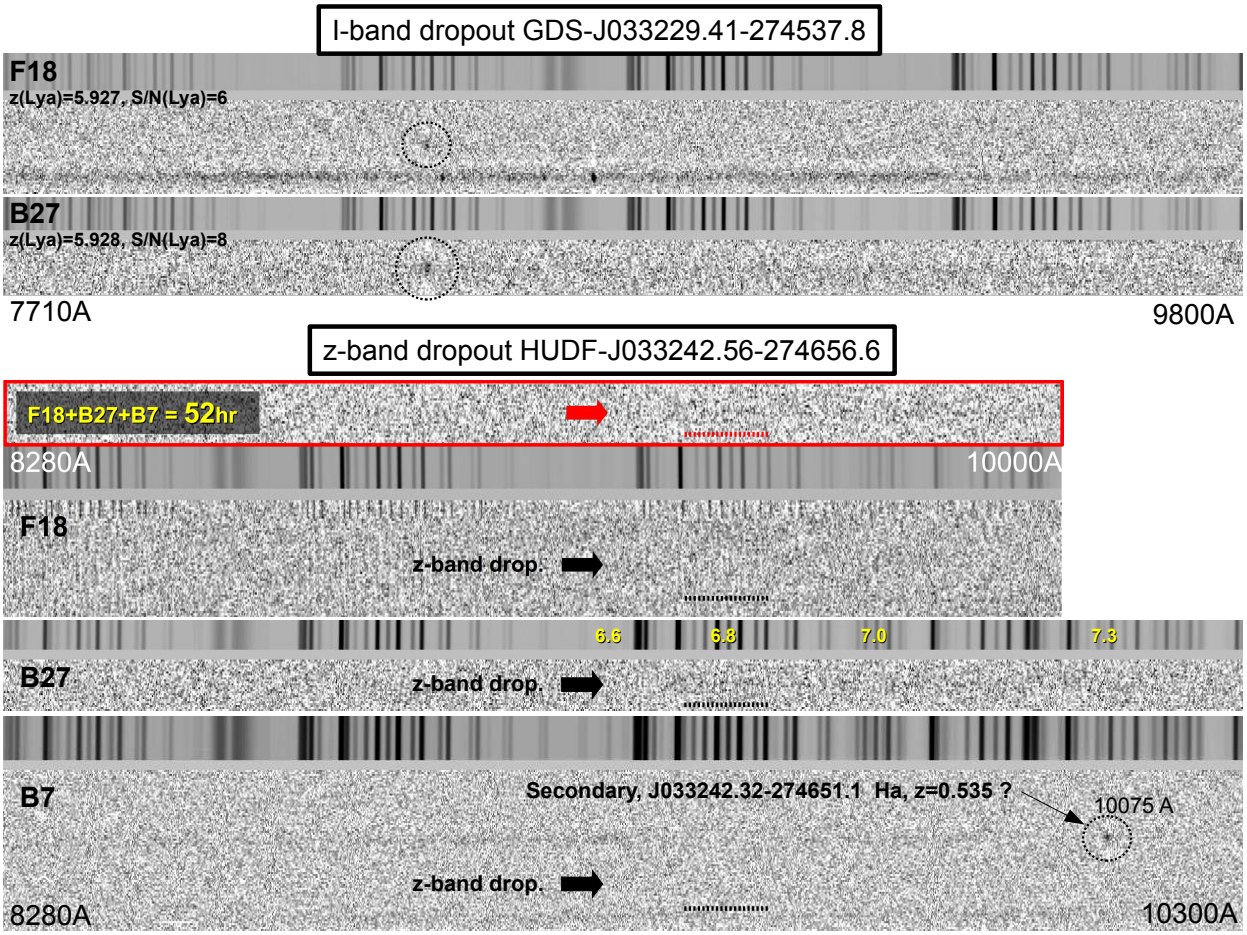

Fig. 1. Two-dimensional signal-to-noise spectra and sky spectra of the galaxies discussed in the text. *Top*: spectra of the *i*-band dropout GDS J033229.41-274537.8 observed in F18 (upper part) and B27 (lower part). The Lyα line is marked with a dotted circle. *Bottom*: stacked 52 h spectrum of the *z*-band dropout G2_1408 is shown with the individual spectra of F18, B27, and B7 (lower part). The expected position of the Lyα continuum break is marked with dotted horizontal lines (see text). In the B27 spectrum the redshift values are reported above the sky as a reference. In the F18 spectrum, the dotted circle marks the older (here revisited) feature discussed in Fontana et al. (2010). The B7 spectrum shows also the Hα emission from the secondary object J033242.32-274651.1 at $z = 0.535$, which is useful here as an example of a still performing FORS + 600*z* configuration beyond one micron.

corresponding to a redshift of 6.972 that we reported in Fontana et al. (2010) with $S/N < 7$ (and shown with a circle in the F18 spectrum of Fig. 1). Exploiting the rms map we derived, the reliability of the spectral feature in the F18 spectrum turns out to have $S/N \simeq 4.5$. In the combined (52 h) spectrum, however, the S/N at the same wavelength position is even smaller, $\lesssim$3, and suggests that the earlier tentative detection was most probably a noise spike.

To assign a statistical significance to our 52 h non-detection, we estimated the minimum line flux that is reachable with the deep FORS2+600z spectrum by computing simulations, as in V11 and P14. Two-dimensional asymmetric Lyα lines have been inserted in the raw science frames, which move the line from $z = 5.7$ to 7.3 with d$z = 0.0013$ (i.e., one pixel at the given spectral resolution). This includes the dithering pattern, varying the FWHM and the line flux, and convolving with spectral resolution along the dispersion and with the seeing along the spatial direction (extracted from the header of each science frame). Knowing the exact position of the inserted lines in the raw frames (which include the cosmic rays by definition), and including the full reduction pipeline process and the response curve, we can reliably access the limits attainable by the instrument. The resulting S/N of the simulated lines are fully compatible with those we observed at redshift 6 and 7 (P11, P14, and V11).

The upper limit we derive from the combined 52 h spectrum is $f(\mathrm{Ly}\alpha) < 3 \times 10^{-18}$ erg/s/cm^2 at three-sigma (in the sky-lines) and up to nine-sigma (in sky-free regions) in the whole wavelength range, up to $z = 7.0$ (see Fig. 4). Adopting the $F125W = 26.10 \pm 0.02$ as the estimation of the continuum under the Lyα line and given the relatively flat UV slope in the near-infrared bands, the limit on the Lyα flux corresponds to an upper limit on the equivalent width $EW < 9$ Å with the same statistical accuracy. It represents the faintest limit on the Lyα flux ever derived at $z > 6.5$.

While absorption lines are clearly impossible to detect in our spectra, it is worth to investigating whether the non-detection of the continuum in the 52 h spectrum is compatible with the expected magnitude $\simeq$26.1. With this aim, a set of two-dimensional continua (with a flat UV slope) without any absorption line have been added to the raw frames as performed for line simulations, by adopting a Gaussian profile in the spatial direction (consistent with the observed seeing). They have been added to the raw frames with dithering and dimmed in magnitude from 23.0 to 27.0 with d$m = 0.25$. In all processes, the response curve has been taken into account. Figure 4 shows the results. The S/N decreases accordingly with the magnitude dimming and in the presence of sky emission lines, becoming impossible to detect at a magnitude $\simeq$26.0 unless the object is at redshift below 6.6

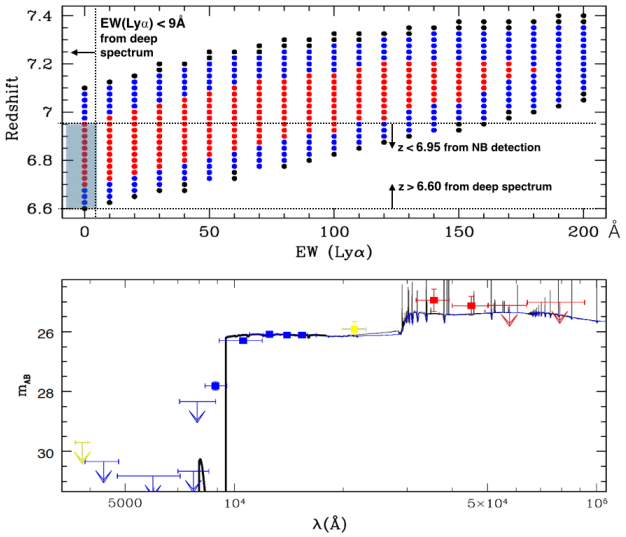

Fig. 2. *Top*: projected Redshift-EW(Lyα) solutions of the SED fitting are shown. Black, blue, and red symbols represent three-,two-, and one-sigma solutions. The well-detected signal in the z_{850}-band is reproducible with a large EW(Lyα) at a higher redshift ($z > 7$) or very faint Lyα emission at the lower redshift, $z < 7$. Upper and lower horizontal dotted lines mark the limits provided by the NB973 detection and non-continuum detection below $z = 6.6$ in the deep spectrum, respectively. The vertical dotted line marks the upper limit of the Lyα rest-frame equivalent width. The transparent gray region underlines the most probable redshift interval. *Bottom*: SED fitting performed with BC03 libraries with (thin black) and without (blue) nebular emission lines are shown. The fit to the HST bands only is shown with the thick black line. Blue, yellow, and red points represent photometry from HST, VLT (U and K bands), and *Spitzer*/IRAC, respectively. Upper limits at one sigma are marked with arrows.

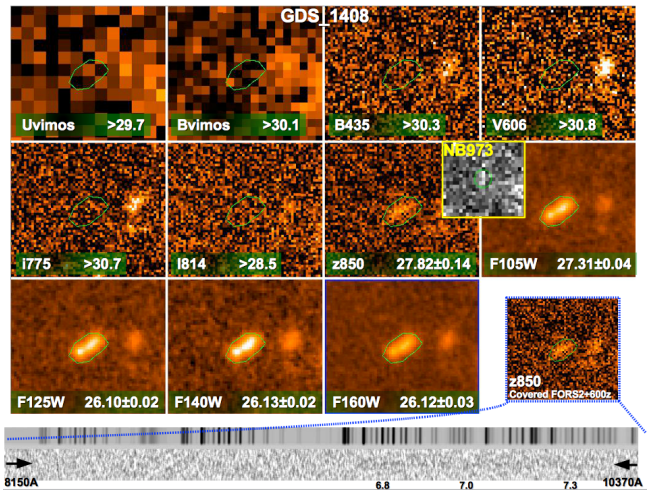

Fig. 3. Cutouts ($3'' \times 3''$) from U to H-band of G2_1408 are shown with the magnitudes (limits are at one-sigma). The green contour marks the galaxy's shape as a guidance. The inset image placed between the z_{850} and $F105W$ refer to the narrow band filter NB973 in which the source is detected (three-sigma). The bottom-right cutout shows the clear detection in the z_{850} band ($S/N \sim 8$), for which there is a good coverage of the ultradeep FORS2 spectrum (also reported in the bottom).

(see Fig. 4). Both simulations on Lyα line and continuum show the clear decrease of the S/N at the position of sky emission lines, in which it is lower where the sky emission is stronger. The results of the continuum simulation are in line with the observed faint galaxies, especially with those we confirmed in P11 at $z \sim 6$ based on continuum-break only.

3.2. Refined redshift

Depending on its equivalent width, the Lyα emission can contribute significantly to broadband photometry, as a consequence to the photometric redshift determination. In particular, the flux observed in the z_{850} band (see Fig. 3) depends on the position of the Lyα-line/break (i.e., the redshift), the IGM attenuation, the EW of the possible Lyα emission (EW(Lyα)), and mildly on the UV slope of the source, β ($F_\lambda = \lambda^\beta$). With the depth and photometric quality available for this galaxy and the upper limit derived above, the redshift value can be refined. With this aim we performed the SED fitting with Bruzual & Charlot (2003, BC03, hereafter) templates by including different equivalent widths of the Lyα (0–200 Å rest-frame) and focusing solely on the break between the optical and near-infrared bands, which include B_{435}, V_{606}, i_{775}, z_{850}, $F105W$, $F125W$, $F140W$, and $F160W$. We have not included the NB filter in this exercise since its photometry is not as accurate as the HST data. The templates adopted a range of e-folding star-formation timescales ranging from 0.1 to 15 Gyr (the latter being a constant-star formation history in practice), metallicities from $Z = 0.2\,Z_\odot$ to $Z = Z_\odot$, and a Calzetti attenuation curve with $A_V = 0$–3. Figure 2 shows the *plane* (redshift–EW(Lyα)), in which the degeneracy is clear; that is, a progressively stronger Lyα emission is required at increasing redshifts to compensate for the increasing absorption by the IGM. The degeneracy with the Lyα line is broken by including the result from the ultradeep 52 h spectrum discussed in Sect. 3.1, which forces the EW(Lyα) to be smaller than 9 Å rest-frame. Once the Lyα constraints are included, the redshift of G2_1408 is constrained within 6.7 and 6.95 at 1σ and 6.6 and 7.1 at 2σ. The top panel of Fig. 2 shows the resulting region where the redshift would lie, that is $z = 6.82^{+0.1}_{-0.1}$ (at one sigma).

We note that the 2σ range is consistent with the continuum-only simulations as described above and the non-detection in the sky-free region of the spectrum at 9000 Å $< \lambda <$ 9280 Å, *where both* suggest a lower limit of the redshift, $z_{\rm MIN} = 6.6$. Less significant but consistent with $z_{\rm MIN}$, is the slightly brighter 3.6 μm magnitude with respect to the 4.5 μm channel in the data we have, which could suggest a flux boost of the [OIII]4959–5007+Hβ structure in the first channel, while the $H\alpha$ line is outside (redward) the second one, respectively. Indeed, this is confirmed with deeper IRAC data, in which a clear break has been measured, [3.6–4.5] μm = 0.66 ± 0.2 (Smit et al., in prep., Labbé et al. 2013). This is fully consistent with our redshift estimation.

The SED fitting with and without the nebular component has then been performed by including the IRAC and ground based photometry. We have included the full treatment of the nebular emission (both in lines and continuum), which is computed using the Schaerer & de Barros (2009) model, as described in Castellano et al. (2014). The resulting SED fits with HST-only bands, and the entire photometry are shown in the bottom panel of Fig. 2. The derived physical quantities in the various cases agree within a factor of two. This exercise provides an estimate of the stellar mass of $M = 5^{+3}_{-2} \times 10^9 M_\odot$, an age of $\simeq 0.1^{+0.15}_{-0.05}$ Gyr, a dust attenuation $E(B-V)$ of $\simeq 0.1 \pm 0.05$, and a dust corrected star formation rate of $21^{+20}_{-10}\ M_\odot\ {\rm yr}^{-1}$.

4. Discussion

The combination of excellent photometry and ultradeep spectroscopic data leads us to conclude that the lack or extreme

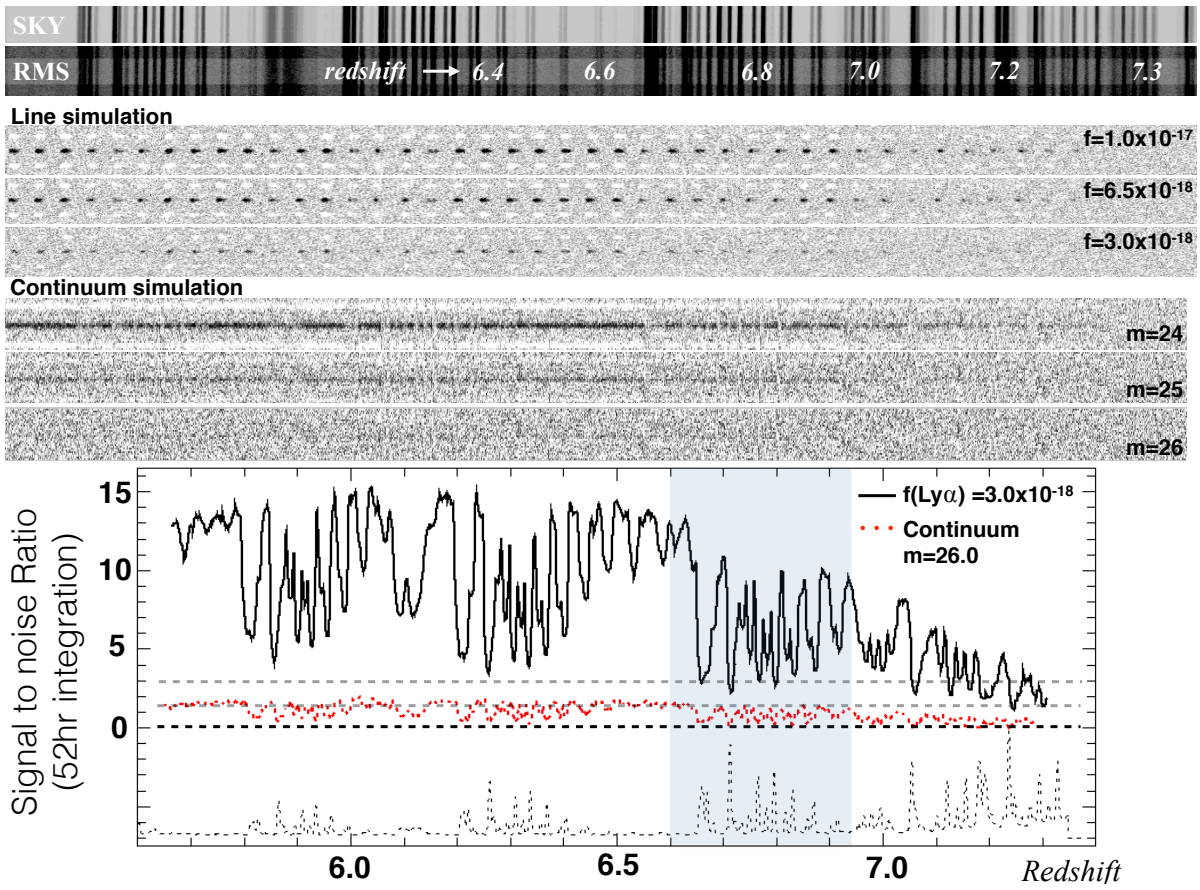

Fig. 4. Simulation of the expected signal-to-noise ratio for emission Lyα line and continumm with a 52 h integration with FORS2. *From top to bottom*: the two dimensional spectra of the sky and RMS map are shown as an example and guidance for the eye. Simulated signal to noise 2d-spectra of line emission (snapshot) and continuum emissions are shown with an indicated line flux and magnitude at the (flat) continuum on the right. It is clear that the S/N is lower where the sky lines are stronger. In *the bottom part* the S/N of the Lyα feature versus redshift (solid black line) and the continuum (red dotted line) are reported for the case of GDS_1408. The transparent grey region marks the $z_{\rm MIN} < z < z_{\rm MAX}$ interval; see text for more details. Grey horizontal dotted lines mark $S/N = 1.5$ and 3.0.

weakness of a Lyα emission is a real feature of this object. It is therefore worth investigating the reasons why the Lyα line is not present.

4.1. The effective Lyα escape fraction

Dijkstra & Jeeson-Daniel (2013) differentiate between the term "escape" fraction and "effective escape" fraction of Lyα photons, $f_{\rm esc}$(Lyα) and $f_{esc}^{\rm eff}$(Lyα), respectively. The former being related to the transport of photons out of the galaxy's interstellar medium, while the latter includes further damping by the IGM, which gives rise to a low-surface-brightness Lyα glow around galaxies. Therefore, $f_{\rm esc}^{\rm eff}$(Lyα) can be much smaller than $f_{\rm esc}$(Lyα). If we assume "normal" metallicities and IMFs, where star formation is ongoing at equilibrium (age $>$ 100 Myr with constant SFR) on average, an estimation of the Lyα luminosity can be obtained by imposing SFR(UV)/SFR(Lyα) $\simeq$ 1 (Hayes et al. 2011; Verhamme et al. 2008). Assuming that the SFR(UV) corrected by dust extinction is representative of the total ongoing star formation activity, the intrinsic Lyα flux turns out to be $\simeq 4 \times 10^{-17}$ erg s^{-1} cm^{-2}, i.e., EW(Lyα) rest-frame $\simeq$120 Å. The upper limit on the observed Lyα line flux derived above corresponds to an observed EW(Lyα) $<$ 9 Å rest-frame (at 3–9σ), 13 times smaller than the expected intrinsic emission, that gives an upper limit of $f_{\rm esc}^{\rm eff}$(Lyα) $<$ 8%.

4.2. What is attenuating the Lyα emission?

The escape of Lyα photons from a gaseous and dusty interstellar medium is a complex process which is sensitive to a number of physical properties, such as dust and gas mass, star formation rate, metallicity, kinematic, escaping ionizing radiation, the gas geometry, and filling factor and the galaxy orientation (Neufeld 1991; Verhamme et al. 2008, 2012; Hayes et al. 2011; Yajima et al. 2014; Laursen et al. 2013; Dijkstra et al. 2014). Additionally, the neutral hydrogen in the IGM can scatter part of the Lyα photons and decrease the line luminosity. For example, Laursen et al. (2011) suggested that the average IGM transmission could be $\simeq$20% at $z = 6.5$. In this case, the transmission is sensitive on the viewing angle and the environments of the galaxy, as it is affected by the inhomogeneous filamentary structure of IGM. At $z > 6.5$ the IGM damping could be the dominant effect.

It is not possible to investigate the above quantities with the current information in detail. Therefore, we have to rely on global properties, such as by performing a comparative analysis with lower redshift galaxies at $z > 3$–4. First, it has been shown that $2 < z < 6$ UV-bright star-forming galaxies ($L > L^\star$) show a deficit of Lyα emission with respect the fainter UV counterparts on average (e.g., Ando et al. 2006; Vanzella et al. 2009; Lee et al. 2013; Balestra et al. 2010). This is consistent with

the interpretation that intrinsically bright galaxies in the UV are also more star forming, massive, and more chemically enriched on average and thus more likely to be obscured by dust, especially the Lyα resonant transition that is expected to be efficiently absorbed. A decreasing trend of $f_{\rm esc}$(Lyα) emission with increasing $E(B-V)$ has also been observed in several studies (Giavalisco et al. 1996; Atek et al. 2008; Verhamme et al. 2008; Kornei et al. 2010; Hayes et al. 2011). The observed UV slope ($\beta = -2$) of GDS_1408 suggests that there is a dust attenuation of $A1600 \sim 1.3$ (Castellano et al. 2014; de Barros et al. 2014). Inferring $SFR \simeq 21\ M_{\odot}\,{\rm yr}^{-1}$ and assuming the Schmidt law (Schmidt 1959; Kennicutt 1998a), a non-negligible amount of gas implies ($M_{\rm gas} \simeq 3 \times 10^9\ M_{\odot}$), a comparable value to the stellar mass and would favor a more efficient Lyα photon destruction operated by dust. The presence of dust and gas would also suggest that the escape fraction of ionizing radiation is very low, as it has been observed in $L^{\star}$ star-forming galaxies at $z \simeq 3$ (Vanzella et al. 2010a; Boutsia et al. 2011).

Second, GDS_1408 is one of the more extended sources among the $z \sim 7$ candidates (half light radius of 0.26″, with an elongated morphology of 4.8×2.5 proper kpc, Grazian et al. 2011, see Fig. 3). It has been shown that the Lyα equivalent width and the size observed at the 1500 Å rest-frame of the stellar continuum anti-correlate, such that the emitters appear more compact and nucleated than the non-emitters on average, with an average half-light radius $\lesssim$1 kpc (Law et al. 2007; Vanzella et al. 2009; Pentericci et al. 2010).

The object GDS_1408 is moderately star forming and contains a non-negligible amount of dust, it is UV bright and spatially extended. While we cannot exclude that the CGM/IGM plays an additional role, the properties of GDS_1408 are consistent with those of other lower-z $L^{\star}$ star-forming galaxies that show faint Lyα emission and is not a "smoking gun" of an increased neutral IGM at $z = 7$. It is worth noting that we are discussing a single galaxy case, which clearly cannot be considered as representative of a population. The deficit of Lyα lines from redshift 6 to 7 recently observed is significant and is based on a statistical analysis that compares tens of star-forming galaxies that are selected with very similar color techniques, which are independent from the presence of the Lyα line. However, as also noted in Schenker et al. (2014), galaxies like GDS_1408 are not the best tracers of an IGM damping. The higher the probability the more Lyα emission is internally absorbed and the lower the power of tracing the neutral gas fraction from the ICM/IGM.

Nonetheless, it is important to assess the nature of "continuum-only" star-forming galaxies at $z > 6.5$, which is still an unexplored line of research. As reported in this work, the tentative spectroscopic investigation of "continuum-only" galaxies at $z > 6.5$ shows all the limitations of the 8-10 meter class telescopes that are coupled with optical spectroscopy ($\lambda < 1.1\ \mu$m). Different and future facilities are needed to shed light on their nature.

4.3. Future prospects: ALMA, JWST, and ELT

We have shown the current limits of 8–10 m class telescopes in the spectroscopic characterization and redshift measurement of non-Lyα emitters at $6.6 < z < 7.3$. If $z \sim 7$ is a critical value above which the visibility of Lyα lines decreases drastically, then future facilities are necessary to capture the UV continuum-break, the ultraviolet absorption lines, and/or optical nebular emission lines at $7 < z < 10$. The JWST-NIRSPEC will probe the typical nebular emission lines, such as [OII]3727, Hβ, [OIII]4959-5007 up to $z \simeq 9$ (5 μm) and the extremely large telescopes (ELT, 30–40 m diameter) will allow us to cover the mid-infrared (e.g., EELT-METIS, 8–14 μm) and to probe the UV continuum with $S/N = 10$ down to $J \simeq 27$. Therefore, we are able to study the ultraviolet absorption lines in detail, not to mention the possibility to perform high spatial resolution analysis.

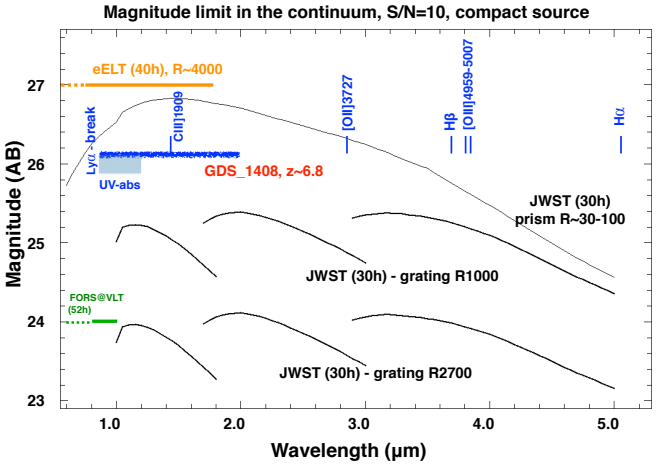

Fig. 5. Expected magnitude limits in the continuum ($S/N = 10$) with 30–50 h integration time are shown for ELT, (orange, Evans et al. 2013), JWST (black, available in tabular form http://www.stsci.edu/jwst/instruments/nirspec/sensitivity/) and a VLT-FORS (green, this work). The estimated limit for KMOS is magnitude ≃21.5 in the YJ band with 50h integration (rescaling from the KMOS manual, Sect. 2.3.4). The schematic position of GDS_1408 is reported (blue) with the continuum magnitude ≃26.1, the typical ultraviolet absorption lines from the Lyα to CIV 1550 (grey region, UV-abs) and the basic emission lines, e.g., CIII]1909, [OII]3727, Hβ, [OIII]4959-5007 and Hα.

In particular, the case of GDS_1408 is shown in Fig. 5, where a schematic view of the limits on the continuum at $S/N = 10$ are reported for the ELT, JWST and VLT telescopes. A good characterization of the ultraviolet absorption lines will be feasible with the ELT. The JWST would marginally identify the trace of the continuum ($S/N < 5$) but will open for the measure of optical emission lines (up to [OIII]4959-5007).

While the JWST and ELT will definitely perform these kind of studies, at present the measure of the redshift with 8–10 m telescopes could be achieved by looking at emission lines different from Lyα. Though unusual, lines like OIII]$\lambda\lambda$1661-1666 and CIII]$\lambda\lambda$1907-1909 could be identified by means of near-infrared spectrograph (e.g., Stark et al. 2014). Moreover, depending on the source of ionizing photons, other lines like NV 1240, NIV]$\lambda\lambda$1483-1486, CIV 1550, and HeII 1640 can also be measured (e.g., Osterbrock & Ferland 2006; Vanzella et al. 2010b; Raiter et al. 2010; Steidel et al. 2014).

Another promising facility that might be able to determine the spectroscopic redshift of this galaxy is ALMA. Indeed, a spectral scan of the [CII]158 μm line encompassing the full 2-sigma range of uncertainty could be covered with two ALMA spectral bands. Assuming that the local SFR-[CII]158 μm relation of Sargsyan et al. (2012) also holds at these high redshifts, we expect a flux of 0.24 Jy km s^{-1} based on the best-fitting $SFR = 20\ M_{\odot}/{\rm yr}^{-1}$, which can be secured in a relatively short time (<6 h in the Cycle2 sensitivity) with ALMA. A molecular line scan that covers the 3 mm window (89–115 GHz) can also reveal multiple CO transitions in GDS_1408. In particular at $z > 6.5$ the transitions $J = 7 \rightarrow 6$ and $J = 6 \rightarrow 5$ (where J is the

rotational quantum number) are observable. Given the UV slope and the star formation activity and assuming the relation between CO line luminosity and SFR (see Carilli & Walter 2013; Decarli et al. 2014), the expected CO transitions can be detected ($S/N \gtrsim 3$) with an ALMA 3 mm scan with a sensitivity limit of 0.1 mJy beam^{-1}.

5. Conclusions

We have reported on the combined VLT/FORS2 spectroscopy of one of the most reliable $z \simeq 7$ galaxy candidates in the *Hubble* Ultra Deep Field. Three different programs at VLT targeted GDS_1408 in the last five years, for a total integration time of 52 h. From the ESO archive we have retrieved all these data, and re-analyzed them in a consistent way. Our main results are:

1. *An upper limit on the Lyα emission*: we are able to place a stringent upper limit of $f(\mathrm{Ly}\alpha) < 3\times10^{-18}$ erg/s/cm^2 at three-sigma (in the sky-lines) and up to a nine-sigma (in sky-free regions) in the whole wavelength range, up to $z = 7.0$ (see Fig. 4). This corresponds to an upper limit on the equivalent width, $EW < 9$ Å, with the same statistical accuracy. With the deeper data used, we do not confirm the tentative detection of a weak line located at $\lambda = 9691.5 \pm 0.5$ Å, corresponding to a redshift of 6.972, which we claimed in F10.
2. *Redshift refinement*: the combination of ultradeep spectroscopy, superb HST information, and narrow band imaging have allowed us to refine the photometric redshift value of GDS_1408, which turns out to be 6.82 ± 0.1. The same analysis indicates that GDS_1408 has a nearly solar metallicity and is a relatively dust attenuated ($A_{1600} \simeq 1$) galaxy.
3. *Lyα escape fraction*: we derived a $f_{\rm esc}^{\rm eff}(\mathrm{Ly}\alpha) < 8\%$. The Ly$\alpha$ attenuation can be a combination of internal (ISM) and external effects (IGM).

Even though we cannot rule out a major contribution of the IGM in damping the line, the *most* plausible interpretation is that G2_1408 is a star-forming galaxy at $z \simeq 6.82$ that has moderately evolved and contains sufficient gas and dust to attenuate the Lyα emission before it reaches the IGM. If compared with a fainter ($0.05L^\star < L < 0.2L^\star$), younger, less massive and less evolved counterpart that shows Lyα emission and a much steeper UV slope $\beta < -2.5$ (e.g., Balestra et al. 2013; Vanzella et al. 2014), G2_1408 appears more massive and evolved ($\beta \simeq -2$).

An absence of the line due to dust absorption does not contrast recent results on the deficit of Lyα lines, which have been ascribed to a possible increase of the neutral gas fraction of the IGM between $z \sim 6$ and 7 (e.g., P11, P14, Finkelstein et al. 2013). The apparent drop of lines shows evidence based on statistical samples, in which the properties of redshift 6 and 7 galaxies are compared in a differential way and apply similar color selection techniques.

In general, redshift 7 sources, like GDS_1408 and even fainter ones at $J = 27$, will be well studied spectroscopically with ELT and JWST telescopes, especially for the UV absorption lines and nebular (optical) emission lines, respectively. As an example, JWST will provide the systemic redshift from rest-frame optical nebular emission lines (Oxigen, Balmer lines) and the ELT will capture the signature of the ISM in absorption in the rest-frame ultraviolet. This will not be feasible before 2018–2020. Currently, a facility that can provide redshift measures at $z \gtrsim 7$ and characterize the properties of the ISM and stellar population is ALMA (e.g., Inoue et al. 2014). Sources like GDS_1408 with a reliable guess on the redshift value are suitable candidates for the scanning mode of ALMA.

Acknowledgements. We thank R. Bouwens for providing information about the deep IRAC magnitudes of the source and P. Oesch for providing information about the GDS_1408 target in the spectroscopic program 088.A-1008(A). We thank F. Vito, M. Mignoli, A. Cimatti and S. de Barros for useful discussions. Part of this work has been funded through the INAF grants (PRIN INAF 2012). E.V. thanks V. Davide for helping on Figure 1 visualization to be as informative as possible.

References

Ando, M., Ohta, K., Iwata, I., et al. 2006, ApJ, 645, L9
Atek, H., Kunth, D., Hayes, M., Östlin, G., & Mas-Hesse, J. M. 2008, A&A, 488, 491
Atek, H., Kunth, D., Schaerer, D., et al. 2014, A&A, 561, A89
Balestra, I., Mainieri, V., Popesso, P., et al. 2010, A&A, 512, A12
Balestra, I., Vanzella, E., Rosati, P., et al. 2013, A&A, 559, L9
Behrens, C., Dijkstra, M., & Niemeyer, J. C. 2014, A&A, 563, A77
Bolton, J. S., & Haehnelt, M. G. 2013, MNRAS, 429, 1695
Boutsia, K., Grazian, A., Giallongo, E., et al. 2011, ApJ, 736, 41
Bouwens, R. J., & Illingworth, G. D. 2006, Nature, 443, 189
Bouwens, R. J., Illingworth, G. D., Blakeslee, J. P., Broadhurst, T. J., & Franx, M. 2004, ApJ, 611, L1
Bouwens, R. J., Illingworth, G. D., Franx, M., & Ford, H. 2008, ApJ, 686, 230
Bouwens, R. J., Illingworth, G. D., Oesch, P. A., et al. 2011, ApJ, 737, 90
Bouwens, R. J., Illingworth, G. D., Oesch, P. A., et al. 2014, ApJ, submitted [arXiv:1403.4295]
Bruzual, G., & Charlot, S. 2003, MNRAS, 344, 1000
Bunker, A., Wilkins, S., Ellis, R., et al. 2010, MNRAS, 409, 855
Carilli, C. L., & Walter, F. 2013, ARA&A, 51, 105
Caruana, J., Bunker, A. J., Wilkins, S. M., et al. 2014, MNRAS, 443, 2831
Calzetti, D., Armus, L., Bohlin, R. C., et al. 2000, ApJ, 533, 682
Castellano, M., Fontana, A., Boutsia, K., et al. 2010, A&A, 511, A20
Castellano, M., Fontana, A., Grazian, A., et al. 2012, A&A, 540, A39
Castellano, M., Sommariva, V., Fontana, A., et al. 2014, A&A, 566, A19
de Barros, S., Schaerer, D., & Stark, D. P. 2014, A&A, 563, A81
Decarli, R., Walter, F., Carilli, C., et al. 2014, ApJ, 782, 78
Dijkstra, M., & Jeeson-Daniel, A. 2013, MNRAS, 435, 3333
Dijkstra, M., & Wyithe, J. S. B. 2010, MNRAS, 408, 352
Dijkstra, M., Mesinger, A., & Wyithe, J. S. B. 2011, MNRAS, 414, 2139
Dijkstra, M., Wyithe, S., Haiman, Z., Mesinger, A., & Pentericci, L. 2014, MNRAS, 440, 3309
Duval, F., Schaerer, D., Östlin, G., & Laursen, P. 2014, A&A, 562, A52
Evans, C., Puech, M., Barbuy, B., et al. 2013, White paper presented at the Shaping E-ELT Science & Instrumentation
Fontana, A., Vanzella, E., Pentericci, L., et al. 2010, ApJ, 725, L205
Finkelstein, S. L., Papovich, C., Giavalisco, M., et al. 2010, ApJ, 719, 1250
Finkelstein, S. L., Papovich, C., Dickinson, M., et al. 2013, Nature, 502, 524
Giavalisco, M., Koratkar, A., & Calzetti, D. 1996, ApJ, 466, 831
Grazian, A., Castellano, M., Koekemoer, A. M., et al. 2011, A&A, 532, A33
Hayes, M., Schaerer, D., Östlin, G., et al. 2011, ApJ, 730, 8
Inoue, A. K. 2011, MNRAS, 415, 2920
Inoue, A. K., Shimizu, I., Tamura, Y., et al. 2014, ApJ, 780, 18
Kennicutt, R. C., Jr. 1998a, ApJ, 498, 541
Kennicutt, R. C., Jr. 1998b, ARA&A, 36, 189
Kornei, K. A., Shapley, A. E., Erb, D. K., et al. 2010, ApJ, 711, 693
Labbé, I., Bouwens, R., Illingworth, G. D., & Franx, M. 2006, ApJ, 649, L67
Labbé, I., Oesch, P. A., Bouwens, R. J., et al. 2013, ApJ, 777, 19
Laursen, P., Sommer-Larsen, J., & Razoumov, A. O. 2011, ApJ, 728, 52
Laursen, P., Duval, F., & Oumlstlin, G. 2013, ApJ, 766, 124
Law, D. R., Steidel, C. C., Erb, D. K., et al. 2007, ApJ, 656, 1
Lee, K.-S., Dey, A., Cooper, M. C., Reddy, N., & Jannuzi, B. T. 2013, ApJ, 771, 25
Loeb, A., Barkana, R., & Hernquist, L. 2005, ApJ, 620, 553
McLure, R. J., Dunlop, J. S., Cirasuolo, M., et al. 2010, MNRAS, 403, 960
McLure, R. J., Dunlop, J. S., Bowler, R. A. A., et al. 2013, MNRAS, 432, 2696
Miralda-Escudé, J., Haehnelt, M., & Rees, M. J. 2000, ApJ, 530, 1
Nakajima, K., & Ouchi, M. 2014, MNRAS, 442, 900
Neufeld, D. A. 1991, ApJ, 370, L85
Oesch, P. A., Bouwens, R. J., Illingworth, G. D., et al. 2010, ApJ, 709, L16
Ono, Y., Ouchi, M., Mobasher, B., et al. 2012, ApJ, 744, 83
Osterbrock, D. E. 1989, Astrophysics of Gaseous Nebulae and Active Galactic Nuclei (Mill Valley: Univ. Science Books)
Osterbrock, D. E., & Ferland, G. J. 2006, Astrophysics of gaseous nebulae and active galactic nuclei, 2nd edn., eds. D. E. Osterbrock, & G. J. Ferland (Sausalito, CA: University Science Books)

Ouchi, M., Shimasaku, K., Akiyama, M., et al. 2008, ApJS, 176, 301
Pentericci, L., Grazian, A., Scarlata, C., et al. 2010, A&A, 514, A64
Pentericci, L., Fontana, A., Vanzella, E., et al. 2011, ApJ, 743, 132
Pentericci, L., Vanzella, E., Fontana, A., et al. 2014, ApJ, submitted [arXiv:1403.5466]
Raiter, A., Schaerer, D., & Fosbury, R. A. E. 2010, A&A, 523, A64
Rauch, M., Becker, G. D., Haehnelt, M. G., et al. 2011, MNRAS, 418, 1115R
Robertson, B. E., Ellis, R. S., Dunlop, J. S., McLure, R. J., & Stark, D. P. 2010, Nature, 468, 49
Sargsyan, L., Lebouteiller, V., Weedman, D., et al. 2012, ApJ, 755, 171
Schaerer, D. 2003, A&A, 397, 527
Schaerer, D., & de Barros, S. 2009, A&A, 502, 423
Schaerer D., de Barros S., & Stark D. P. 2011, A&A, 536, A72
Schenker, M. A., Stark, D. P., Ellis, R. S., et al. 2012, ApJ, 744, 179S
Schenker, M. A., Ellis, R. S., Konidaris, N. P., & Stark, D. P. 2014, ApJ, submitted [arXiv:1404.4632]
Schmidt, M. 1959, ApJ, 129, 243
Shibuya, T, Kashikawa, N., Ota, K., et al. 2012, ApJ, 752, 114
Siana, B., Teplitz, H. I., Colbert, J., et al. 2007, ApJ, 668, 62
Stark, D. P., Ellis, R. S., & Ouchi, M. 2011, ApJ, 728, L2
Stark, D. P., Richard, J., Charlot, S., et al. 2014, MNRAS, submitted [arXiv:1408.3649]
Steidel, C. C., Rudie, G. C., Strom, A. L., et al. 2014, ApJ, submitted [arXiv:1405.5473]
Treu, T., Trenti, M., Stiavelli, M., Auger, M. W., & Bradley, L. D. 2012, ApJ, 747, 27
Treu, T., Schmidt, K. B., Trenti, M., Bradley, L. D., & Stiavelli, M. 2013, ApJ, 775, 29
Vanzella, E., Giavalisco, M., Dickinson, M., et al. 2009, ApJ, 695, 1163
Vanzella, E., Giavalisco, M., Inoue, A. K., et al. 2010a, ApJ, 725, 1011
Vanzella, E., Grazian, A., Hayes, M., et al. 2010b, A&A, 513, 20
Vanzella, E., Pentericci, L., Fontana, A., et al. 2011, ApJ, 730, 35
Vanzella, E., Guo, Y., Giavalisco, M., et al. 2012, ApJ, 751, 70
Vanzella, E., Fontana, A., Zitrin, A., et al. 2014, ApJ, 783, L12
Verhamme, A., Schaerer, D., Atek, H., & Tapken, C. 2008, A&A, 491, 89
Verhamme, A., Dubois, Y., Blaizot, J., et al. 2012, A&A, 546, A111
Verhamme, A., Orlitova, I., Schaerer, D., & Hayes, M. 2014, A&A, submitted [arXiv:1404.2958]
Yan, H., & Windhorst, R. A. 2004, ApJ, 612, L93
Yan, H., Windhorst, R., Hathi, N., et al. 2010, RA&A, 10, 867
Yajima, H., Li, Y., Zhu, Q., et al. 2014, MNRAS, 440, 776
Wilkins, S. M., Bunker, A. J., Lorenzoni, S., et al. 2011, MNRAS, 411, 23
Zackrisson, E., Inoue, A. K., & Jensen, H. 2013, ApJ, 777, 39